Remote Sensing in Ecology and Conservation
Open Access
ZSL LET'S WORK FOR WILDLIFE

ORIGINAL RESEARCH

Land cover classification of treeline ecotones along a 1100 km latitudinal transect using spectral- and three-dimensional information from UAV-based aerial imagery

Ida Marielle Mienna[1], Kari Klanderud[1], Hans Ole Ørka[1], Anders Bryn[2,3] & Ole Martin Bollandsås[1]

[1]Faculty of Environmental Sciences and Natural Resource Management, Norwegian University of Life Sciences, Box 5003, Ås 1432, Norway
[2]Geo-Ecology Research Group, Natural History Museum, University of Oslo, P.O. Box 1172, Oslo NO-0318, Norway
[3]Division of Survey and Statistics, Norwegian Institute of Bioeconomy Research (NIBIO), P.O. Box 115, Ås NO-1431, Norway

Keywords
Drone, EcoSyst, multi-site, spatiotemporal variation, UAV, vegetation

Correspondence
Ida Marielle Mienna, Faculty of Environmental Sciences and Natural Resource Management, Norwegian University of Life Sciences, Box 5003, 1432 Ås, Norway.
E-mail: idmi@nmbu.no

Editor: Temuulen Sankey
Associate Editor: Angela Harris

Received: 10 November 2021; Revised: 25 January 2022; Accepted: 8 February 2022

doi: 10.1002/rse2.260

Remote Sensing in Ecology and Conservation 2022;**8** (4):536–550

Abstract

The alpine treeline ecotone is expected to move upwards in elevation with global warming. Thus, mapping treeline ecotones is crucial in monitoring potential changes. Previous remote sensing studies have focused on the usage of satellites and aircrafts for mapping the treeline ecotone. However, treeline ecotones can be highly heterogenous, and thus the use of imagery with higher spatial resolution should be investigated. We evaluate the potential of using unmanned aerial vehicles (UAVs) for the collection of ultra-high spatial resolution imagery for mapping treeline ecotone land covers. We acquired imagery and field reference data from 32 treeline ecotone sites along a 1100 km latitudinal gradient in Norway (60–69°N). Before classification, we performed a superpixel segmentation of the UAV-derived orthomosaics and assigned land cover classes to segments: rock, water, snow, shadow, wetland, tree-covered area and five classes within the ridge-snowbed gradient. We calculated features providing spectral, textural, three-dimensional vegetation structure, topographical and shape information for the classification. To evaluate the influence of acquisition time during the growing season and geographical variations, we performed four sets of classifications: global, seasonal-based, geographical regional-based and seasonal-regional-based. We found no differences in overall accuracy (OA) between the different classifications, and the global model with observations irrespective of data acquisition timing and geographical region had an OA of 73%. When accounting for similarities between closely related classes along the ridge-snowbed gradient, the accuracy increased to 92.6%. We found spectral features related to visible, red-edge and near-infrared bands to be the most important to predict treeline ecotone land cover classes. Our results show that the use of UAVs is efficient in mapping treeline ecotones, and that data can be acquired irrespective of timing within a growing season and geographical region to get accurate land cover maps. This can overcome constraints of a short field-season or low-resolution remote sensing data.

Introduction

The world's vegetation is changing faster than ever (Mottl et al., 2021), in particular at high latitudes and in alpine regions (Pepin et al., 2015; You et al., 2021). Mapping the distribution of vegetation can aid monitoring changes, improve nature management and increase our knowledge about structural patterns in nature. Forests are expected to expand into open, alpine landscapes with climate warming. Changes in the transition zone between the upper forest boundary and tree-less alpine vegetation (i.e. treeline ecotones) influence the coupling between land and atmosphere. By substantially changing albedo, heat storage, evapotranspiration and carbon sequestration,

elevational shifts in treeline ecotones can alter climate conditions and feedbacks on regional to global scales (Mooney et al., 2020; Ramtvedt et al., 2021; Rydsaa et al., 2017). Elevation-dependent warming will amplify changes in treeline ecotones (Pepin et al., 2015). Thus, monitoring land cover changes in treeline ecotones is important.

Many treeline studies have focused on the temporal changes of treeline position (e.g. Bryn & Potthoff, 2018; Hofgaard et al., 2013), but few have studied the spatial distribution of the treeline ecotone vegetation and tree development (but see Mienna, Speed, Klanderud, et al., 2020). Indeed, a review found that parallel with global warming, only around half of treelines in the world have shown an upward shift in the last century (Harsch et al., 2009), suggesting other factors than climate are affecting treeline dynamics. Several studies have found plant–plant interactions to be important for tree recruitment in treeline ecotones (e.g. Batllori et al., 2009; Loranger et al., 2017; Mikola et al., 2018), and in some cases also more important than climate (Neuschulz et al., 2018; Tingstad et al., 2015). Different vegetation covers may give dissimilar conditions for tree germination and growth, where, for example open terrain can give more thermally positive effects than closed montane forests (Körner, 2012). Thus, to predict tree recruitment, survival and growth in treeline ecotones over time, we need process-understanding and relevant wall-to-wall (i.e. complete coverage) information about land cover and other site-specific variables.

One way to achieve wall-to-wall land cover information is through remote sensing. Imagery acquired from sensors mounted on satellites, aircrafts and unmanned aerial vehicles (UAVs) provide opportunities for land cover mapping over various spatial extents and with various spatial resolutions. Although land covers can be classified through field-based mapping, remote sensing can provide the basis for a more consistent and cost-efficient mapping method (Borre et al., 2011; Haga et al., 2021). Land cover mapping through remote sensing has most frequently been carried out using satellite and aerial images because of their capability to cover vast areas (Cihlar, 2000). However, images captured by these platforms have relatively low spatial resolution (e.g. 0.1–1 m for manned airborne and 0.5–5 m or lower for spaceborne) or are taken at times that are not necessarily optimal for land cover mapping. On the other hand, imagery from UAVs can have ultra-high spatial resolution with pixel-sizes on cm-level, making it possible to map smaller objects such as individual plants (Hamylton et al., 2020). In addition, UAVs can be used to overcome spatiotemporal mismatches between field and remote sensing data (Gonzalez Musso et al., 2020; Shahbazi et al., 2014).

In addition to high spatiotemporal resolution, UAVs can be used to acquire many of the same remotely sensed variables as can be achieved from sensors mounted on manned airborne and spaceborne platforms. High spectral resolution can improve plant community mapping by giving rise to various vegetation indices (Villoslada et al., 2020) or individual species' spectral signatures (Sankey et al., 2018). Three-dimensional data from lidar sensors and Structure-from-Motion can give information about vegetation height and structure (Puliti et al., 2019), which can be useful in land cover classifications (Al-Najjar et al., 2019). Highly fragmented landscapes such as peatlands (Rasanen et al., 2019) and bog-heathland mosaics (Díaz-Varela et al., 2018) have successfully been mapped for vegetation composition using UAVs. For treeline ecotone mapping, satellite or aerial imagery have been the most common platforms (Morley et al., 2018). Treeline ecotone vegetation can, however, vary over short distances and be very fragmented (Ullerud et al., 2016), and UAV imagery with ultra-high resolution can have certain benefits over other platforms with lower resolution. The use of UAVs for biodiversity monitoring and detection of land cover change can thus potentially be a better solution than using imagery from spaceborne or manned airborne platforms taken at unfavourable times (Blackburn et al., 2021; Getzin et al., 2012; Woellner & Wagner, 2019).

Acquiring UAV imagery for monitoring land cover change is not without challenges. Plant communities at higher elevations and latitudes have relatively short growing seasons. Changes in phenological state throughout the growing season can give higher spectral variation than preferred (Wang & Gamon, 2019). Thus, obtaining UAV imagery for multiple treeline ecotone sites at different times during the growing season and in different geographical regions, might affect the land cover classification accuracy. In addition, data acquisition under different weather conditions and timing of the day can have an impact on the UAV imagery due to wind, cloudiness and solar angle, leading to variations in shadows, illumination and blurriness (Yao et al., 2019). Thus, the importance of acquiring imagery under similar conditions has been stressed (Müllerová et al., 2017; Prosek & Simova, 2019). However, alpine sites are often not easily accessible, and thus neither the optimal weather, timing of the day nor season might be possible to achieve. It is therefore important to investigate if land cover maps can still be made with adequate accuracy across multiple sites distributed over large areas, even if the conditions are not optimal.

In this study, we evaluate the potential for land cover mapping of multiple treeline ecotone sites in Norway using ultra-high spatial resolution UAV imagery. Using

field data acquired from sites located along a 1100 km long latitudinal transect, we investigate the influence of acquisition time during the growing season and geographical variation on the applicability of the methods. Furthermore, we examine which remote sensing-derived features to select to increase land cover map accuracy in the treeline ecotone.

Materials and Methods

Study area

The treeline ecotone sites used in this study are situated along a latitudinal transect from 60 to 69°N in Norway (Fig. 1A, Table S1). The sites were originally used to sample field data as ground reference for tree detection by airborne laser scanning (ALS) along the same transect (Thieme et al., 2011). The sites range from 350 to 1200 m above sea level (a.s.l.) and the treeline ecotones vary from being abrupt to gradual to patchy. More background information about the transect and study sites can be found in Thieme et al. (2011) and Mienna, Speed, Klanderud, et al. (2020). In this study, we collected field reference and UAV data in three periods during the growth season of 2018: early (July 2nd–July 14th), mid (August 6th–16th) and late (September 4th–12th). We visited each site only once and thus have one drone campaign per site. The sites are located in three geographical

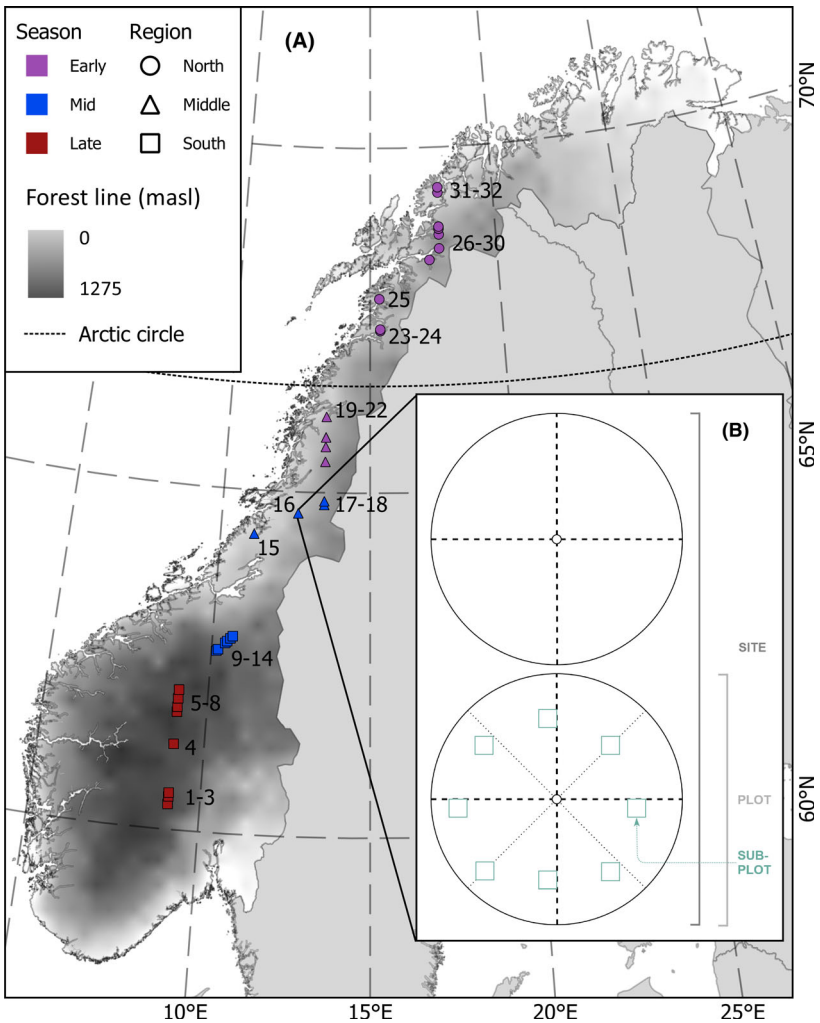

Figure 1. (A) Map showing the 32 sites in Norway where we collected data. The sites are coloured by data acquisition time in the season: early, mid, and late. The three different symbols represent the three geographical regions that we acquired data from: north, middle, and south. The sites are numbered by map ID as found in Table S1. Background map shows empirical forest lines in Norway in meters above sea level and is adapted from Bryn & Potthoff (2018). (B) Sampling design within each site showing plots with quadrants where we recorded trees and sub-plots where we recorded vegetation data.

regions in Norway: south, middle and north (Fig. 1). The southern region has a more continental climate than the two other regions, with less annual precipitation and colder winters (Moen, 1998). In addition, this region has treelines with the highest elevation in Norway (>1000 m a.s.l.). The middle and northern region are more oceanic than the southern region, and thus have milder winters and moderate amounts of snow. The northern region is north of the Arctic circle, and has more hours with daylight than the two other regions. The transect originally consists of 36 treeline ecotone sites covering the three geographical regions. However, for four sites we did not obtain UAV imagery due to weather conditions with heavy rain or strong wind (>12 m/s). Thus, data from 32 treeline ecotone sites were used in this study.

Data collection

Reference data

To create land cover maps, we acquired reference data for the UAV imagery at the sites. At each site, we established a transect consisting of two to six 25 m radii plots at 50 or 100 m intervals (Fig. 1B). The transect and plots were distributed to cover the whole treeline ecotone, including forested areas to open, alpine landscape. To record land cover data, we established eight 1 × 1 m sub-plots per plot where the north-eastern corner was 9 m away from the plot centre (Fig. 1B). When in the field, we recorded by visual estimation within each sub-plot the per cent cover of trees, evergreen and deciduous dwarf shrubs, forbs, graminoids, mosses, lichens and dead material (rock, bare soil, litter), and listed names of all vascular plant species present. We also recorded vegetation height and soil depth for four points within each of the sub-plots. In addition, we photographed each sub-plot to assist in the classification of land cover classes.

In addition to registering land cover class within the sub-plots, we registered trees within the plots using point-centred quarter sampling (Warde & Petranka, 1981). Using this procedure, we recorded the tree closest to the plot centre for each of the four quadrants (Fig. 1B). Originally, this procedure was used to register trees for three height classes: ≤1, 1–2 and ≥2 m. However, for this study, we only used data for ≥2 m trees since trees of this height often is used to depict the elevation of Scandinavian treelines (Dalen & Hofgaard, 2005; Halvorsen et al., 2020; Kullman, 1979; Speed et al., 2010). For more details on tree data sampling, see Thieme et al. (2011). To record the high-precision geographical coordinates of vegetation sub-plots and trees, we used survey-grade Global Navigation Satellite Systems (GNSS) receivers (Legacy E+, Topcon, Livermore, CA, USA) in real-time kinetic mode with an expected coordinate precision of around 3–4 cm.

UAV image survey and processing

We acquired UAV imagery using a fixed-wing Sensefly eBee and two cameras: Sensefly S.O.D.A. and Parrot Sequoia. The Sensefly S.O.D.A. camera captures images with a 20-megapixel resolution for three bands (red, green and blue). The Parrot Sequoia camera captures four bands (green, red, red-edge and near-infrared [NIR]) with 1.2-megapixel resolution. We used eMotion 3 to execute the flight missions. The UAV flight plans consisted of perpendicular flight lines with 80% lateral and longitudinal overlap and a flight altitude of 120 m above ground level. To improve the xyz-position of the image, we also placed 5–7 orange wooden crosses (30 cm width) as ground control points (GCPs), which were positioned using the GNSS equipment. Due to eBee platforms only having space for one camera at a time, we flew each flight mission twice. We performed a radiometric calibration of the Parrot Sequoia camera before each flight mission using the provided calibration target. We flew all flight missions between 8:30 and 16:00, with most of the flights flown before noon (Table S1). The weather conditions for each site were in general cloudy (Table S1).

To create point clouds and orthomosaics from the UAV image survey of each site, we used the photogrammetry software Agisoft photoscan v. 1.4.3. To match the images, we used all bands for the Sensefly S.O.D.A. camera and the red-edge and NIR bands for the Parrot Sequoia camera. We manually placed geolocated markers in each image containing GCPs. For image alignment, we chose a high accuracy, key point limit of 40, tie point limit of 4 and adaptive camera model fitting. We created dense point clouds with medium quality and mild depth filtering. From the dense point clouds, we created a digital elevation model, which we further used to create orthomosaics. We cropped the point clouds and orthomosaics by a 50 m buffer around the plots to be used for further analyses. The average point density was 95.4 and 5.3 p m^{-2} for the Sensefly S.O.D.A. and Parrot Sequoia point clouds respectively. The average ground resolution was 3.2 and 12.9 cm/pixel for the Sensefly S.O.D.A. and Parrot Sequoia orthomosaics respectively. More details about point clouds and orthomosaics per site can be found in Table S1.

We created normalized UAV point clouds (nPCs) using a digital terrain model (DTM) made from ALS. We chose to use an ALS-derived DTM due to ALS having higher vertical accuracy than a non-ALS-derived DTM (White et al., 2013). The ALS data mainly came from the National detailed elevation model (NDH) program,

managed by the Norwegian Mapping Authority. However, not all sites were covered by NDH, and we therefore instead used ALS data sampled along the latitudinal transect for these sites (Thieme et al., 2011). To ensure that the vertical information from the nPCs was comparable between sites, we adjusted the nPCs' vertical information by adding the average vertical difference between the UAV point cloud and ALS DTM for known terrain points.

Segmentation and classification

Superpixel segmentation

Before classification, we segmented the SenseFly S.O.D.A. orthomosaics per site into superpixel objects. Superpixels are groups of pixels with similar values, which can be used in the classification instead of the original pixels (Stutz et al., 2018). Because UAV imagery has ultra-high spatial resolution, segment-based classification is often better than pixel-based classification when it comes to computation time and result (Blaschke et al., 2014; Hussain et al., 2013). For this study, we performed the segmentation using simple linear iterative clustering (SLIC) and affinity propagation (AP) clustering (henceforth called SLICAP) (Zhou, 2015). This method performs the segmentation in three steps: (1) the image is segmented into superpixels with SLIC, (2) a similarity matrix is created based upon the superpixels and (3) superpixels with similar properties (here: similarities in the RGB bands) are merged through AP clustering. With SLICAP, the user does not have to choose the number of clusters as this is done in the AP clustering (Zhou, 2015). To segment the orthomosaics into superpixels, we used the function *Image_Segmentation* in the R package *SuperpixelImageSegmentation* (Mouselimis, 2021). In the superpixel segmentation function there are multiple parameters that can be edited by the user. For this study, we chose to have 20 000 superpixels and a colour radius of 5 to get a more detailed segmentation result. To construct the similarity matrix, we chose the median value of each superpixel, and to save computation time, we normalized the constructed similarity matrix before running the AP clustering. The final segmented orthomosaics had an average superpixel size of 1.33 m^2 (min–max: 0.0003–386.74 m^2).

Land cover classes

To classify the treeline ecotone sites, we used the EcoSyst framework (Halvorsen et al., 2020). In Norway, this system is used to classify and map all terrestrial, limnic and marine areas. The framework is based on ecological gradient theory and is used to define land cover classes based on plant species composition and the processes that regulate their distributions. Variation in structure and composition of different abiotic and biotic components, along environmental gradients, is used to systematize ecosystems into different classes. Each land cover class is mutually exclusive, and the classes are intended to embrace all areas and surface categories that exist in Norway (Halvorsen et al., 2020).

Focusing on the treeline ecotone where the forest might expand into, we identified six land cover classes from the EcoSyst framework in our reference data: wetland and five classes within the ridge-snowbed gradient (Table 1). Wetlands are waterlogged areas that commonly are divided into classes like bog, fen, marsh and swamp. However, due to the low number of wetland observations (Table 1), we merged the classes into one main class. Common wetland species in the treeline ecotone are *Rubus chamaemorus* and different *Carex* and *Eriophorum* species. The ridge-snowbed gradient consists of five classes from three major types (exposed ridge, arctic-alpine heath and lee side and snowbed), which are structured by snow cover duration and wind exposure. The ridges are usually covered by lichens, such as *Cetraria nivalis* and *Flavocetraria cucullata*, which are adapted to high wind exposure, drought and thin snow cover. Xeric heath is dry, but less wind-exposed and with a more constant snow cover than ridge. Typical species is the lichen *Cladonia stellaris*, but xeric heath can also have a high cover of the dwarf shrub *Empetrum nigrum*. Sub-xeric heath is dominated by dwarf shrubs, such as *E. nigrum* and *Calluna vulgaris*, but with intrusions of various *Cladonia* lichens and mosses. The lee sides have a thicker snow cover that protects the plants from winter damage and provides available soil moisture throughout the growing season. Lee sides are dominated by dwarf shrubs, such as *Betula nana* and *Vaccinium myrtillus*, usually with grasses and forbs like

Table 1. Land cover classes and number of segments of each class.

Type	Class	Number of segments
Non-vegetation	Rock	272
	Water	184
	Snow	22
	Shadow	128
Vegetation	Wetland	61
	Tree-covered area	190
	Ridge-snowbed gradient	
	Ridge	91
	Xeric heath	65
	Sub-xeric heath	111
	Lee side	302
	Snowbed	99
		Total: 1529

Avenella flexuosa and *Solidago virgaurea*. The snowbeds are abundant in landscape depressions where snow accumulates, thus making the growing season short with high soil moisture. Snowbeds are usually dominated by mosses or by high cover of the grass *Nardus stricta* or the dwarf shrub *Salix herbacea*. We also identified one vegetation class outside of the EcoSyst-framework: tree-covered area. In this study, we define tree-covered areas as trees ≥2 m in height, with typically *Betula pubescens* ssp. *czerepanovii* being the dominating species, but other tree species like *Picea abies*, *Pinus sylvestris*, *Sorbus aucuparia* and *Populus tremula* are common. In addition to classes with vegetation, we had four non-vegetation classes: rock, snow, water and shadow.

To perform the classification, we used the reference data to assign land cover classes to segments. First, we manually classified the sub-plots into one of the land cover classes using the EcoSyst framework description of each class (Halvorsen et al., 2020). Then, we assigned the sub-plot's land cover class to the segment that overlapped the most with the sub-plot. Using ground-truth data on trees ≥2 m in height, we classified segments with coordinates of these trees as being tree-covered areas. If trees and plots occupied the same segment, we classified the segment as tree-covered area. In addition, we manually classified 602 non-vegetation segments as rock, water, shadow and snow using the UAV imagery as reference.

Classification features

To classify the land cover, we generated a total of 29 classification features grouped into five types: spectral, texture, vertical, terrain and shape (Table 2). We calculated spectral features by taking the mean and standard deviation of the five bands red (R), green (G), blue (B), red-edge (RE) and NIR within each segment. In addition to the spectral bands, we calculated two vegetation indices. We calculated Lichtenthaler index 3 (Lic3), which measures the ratio between the B and RE bands (=B/RE) (Lichtenthaler, 1996). Due to the B and RE bands coming from different sensors with different spatial resolutions, we calculated Lic3 using the mean band values for each segment. We also calculated the normalized difference vegetation index (NDVI) using the mean R and NIR bands for each segment as these two bands also were from different sensors (=(NIR − R)/(NIR + R)) (Rouse et al., 1974). For the texture features, we calculated two Haralick grey-level co-occurrence matrix (GLCM) sets of texture measures (contrast and entropy) for all five bands using the R package *glcm* (Zvoleff, 2020). These two measures were proposed by Hall-Beyer (2017) as being good features for land cover classifications. For the calculation, we chose a window size of 5 × 5 and 32 grey levels. The final GLCM features represented the mean GLCM metric values per segment. For the vertical features, we calculated the mean, max and SD of the nPC within each segment. Because land cover types in the treeline ecotone often correlate with topography (Brown, 1994), we calculated two terrain features: SAGA wetness index (STWI) and topographical position index (TPI). Both features were derived from the ALS DTM and generated with SAGA-GIS software using default settings. In addition, we calculated two shape features: area and compactness. The area feature represents the segment area in m^2. The compactness feature represents how circular the segment is, and is calculated using the Polsby–Popper test (Polsby & Popper, 1991).

Table 2. Overview of the 29 classification features used in the Random forest models.

Type	Feature	Feature abbreviation
Spectral	Band mean (R, G, B, RE, NIR)	R_mean, G_mean, B_mean, RE_mean, NIR_mean
	Band standard deviation (R, G, B, RE, NIR)	R_SD, G_SD, B_SD, RE_SD, NIR_SD
	Lichtenthaler index 3	Lic3
	Normalized difference vegetation index	NDVI
Texture	GLCM contrast (R, G, B, RE, NIR)	R_glcm_c, G_glcm_c, B_glcm_c, RE_glcm_c, NIR_glcm_c
	GLCM entropy (R, G, B, RE, NIR)	R_glcm_e, G_glcm_e, B_glcm_e, RE_glcm_e, NIR_glcm_e
Vertical	Normalized point cloud height mean	nPC_mean
	Normalized point cloud height max	nPC_max
	Normalized point cloud height standard deviation	nPC_SD
Terrain	SAGA wetness index	STWI
	Topographical position index	TPI
Shape	Compactness	comp
	Area	area

Land cover classification and accuracy assessment

To assess the importance of seasonal and regional similarity in data acquisition, we compared the performance of four sets of classifications: global, season-based, region-based and season-region-based. For the global classification, all observations were used irrespective of seasonal timing and geographical location. For the season-based, region-based and season-region-based classifications, we performed classifications based upon acquisition time

during the growing season (early, mid, late), geographical region in Norway (north, middle, south) and both acquisition time and geographical region respectively (Table 3).

For each of the 12 classifications, we separated observations into two for model training (70%) and validation (30%). We separated the observations through stratified random sampling so that classes were equally represented in the two samples. To classify the segments, we used Random forest (Breiman, 2001), an algorithm that builds multiple classification trees. The number of randomly sampled features at each split (*mtry*) was chosen with respect to the number of features required to have the lowest out-of-bag (OOB) error. We built 10 000 trees, as suggested by Behnamian et al. (2017) for getting stable feature importance values. For classification accuracy assessment, we computed confusion matrices using the validation data where we derived the overall accuracy (OA), producer's accuracy (PA), user's accuracy (UA) and Kappa index. We also calculated a weighted OA (OA_W), weighted PA (PA_W) and weighted UA (UA_W) where we assigned wrongly classified closely related classes (i.e. classes with similarities in species composition that can make it hard to distinguish them) in the ridge-snowbed gradient as being correct classifications. We computed 95% binomial confidence intervals ($p \pm 1.96 \times \sqrt{p \times (1-p)/n}$, where p is the accuracy and n is the number of observations) for OA and OA_W estimates. To test if the OA and OA_W for each classification-set was higher than the global model's OA and OA_W, we performed pairwise binomial tests. To calculate classification accuracies for the season-based models, we merged the three season-based confusion matrices into one matrix. We replicated the procedure for the region-based and season-region-based models. In addition, to assess the importance of each feature on the classification accuracy, we estimated the permutation accuracy importance as follows: first, for each classification tree, the prediction error on the bootstrap sample not used for training is computed. Second, one feature's values are shuffled and the prediction error for this dataset is computed. Then, the difference between the first and the second prediction error is calculated. Here, a feature will be regarded as important if the prediction error of the second dataset increases. Finally, the difference in prediction error between the two is averaged over all classification trees and normalized by the differences' standard deviation. This procedure was done for all features to estimate their importance.

Table 3. Overview of the number of sites per classification.

Global	Season-based	Region-based	Season-region-based
32	Early: 14 Mid: 10 Late: 8	North: 10 Middle: 8 South: 14	Early-north: 10 Early-middle: 4 Mid-middle: 4 Mid-south: 6 Late-south: 8

More information about each site can be found in Table S1.

Results

The four classification-sets showed small variations in accuracies and prediction outcomes (Figs. 2 and 3, Tables S2–S4). For the global model where we used all observations without taking season and region into account, we got an OA of 73.6% (95% confidence interval (CI): 69.3–77.6%) and a Kappa of 0.69. The OA and Kappa of the season-based, region-based and season-region-based classifications were 70.6% (95% CI: 66.2–74.7%) and 0.66, 70.5% (95% CI: 66.1–74.6%) and 0.66, and 73.8% (95% CI: 69.6–77.8%) and 0.70 respectively. The OA of the four classification-sets did not significantly vary from each other (Fig. 3). When we considered closely related classes along the ridge-snowbed gradient as being correct classifications (OA_W), the OA increased for all models (Fig. 3). The global model's OA_W was significantly higher than the regional and seasonal-regional classification-sets' OA_w (Fig. 3).

Detailed classification results for the global model are presented in a confusion matrix (Table 4). In general, there were few misclassifications between the vegetation and non-vegetation classes. The non-vegetation land cover classes (rock, water, snow, shadow) had higher PA and UA than the vegetation classes (Table 4). For the vegetation classes, tree-covered area had the highest PA and UA, while snowbed and wetland had the lowest. For all ridge-snowbed gradient classes, the PA_W and UA_W were in general higher than the classes' PA and UA.

For the global model, the most important features for classifying land cover classes were the two spectral features mean blue (B) and Lic3 with a mean decrease accuracy between 10% and 11% (Fig. 4). The least important feature types were the two segment shape features compactness and area and the terrain feature STWI. The vertical features (mean, max and SD of the nPC) had all intermediate importance of around 3% in mean decrease of accuracy.

Discussion

Using ultra-high spatial resolution imagery from UAVs can aid the mapping and monitoring of changes in the treeline ecotone. In our multi-site study spanning a 1100 km latitudinal gradient, we show that UAV imagery sampled from different seasons and across geographical regions is not a barrier for classifying land cover classes across treeline ecotone sites.

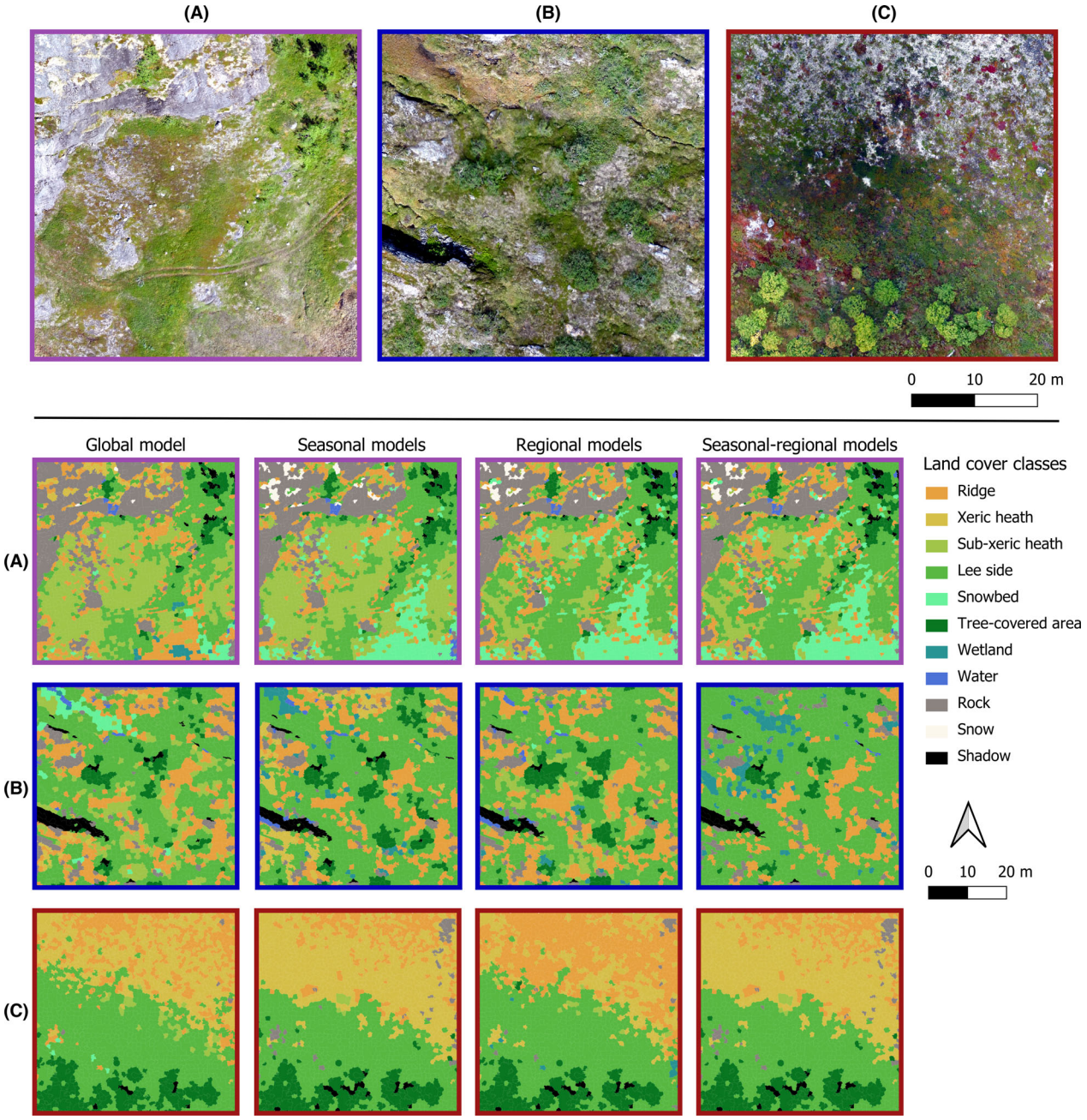

Figure 2. Predicted land cover maps using the global, seasonal, regional and seasonal-regional models for three selected sites. Site A represents data acquired early in the growing season and in the northern region of the transect (map ID 27 as found in Fig. 1 and Table S1). Site B represents data acquired in the middle of the growing season and in the mid region (map ID 18). Site C represents data acquired late in the growing season and in the southern region (map ID 6).

Data acquisition timing and geographical variations

Challenges with the timing of remote sensing data acquisition have been underlined (Müllerová et al., 2017). This is due to various factors, for example phenological effects that can influence remote sensing-derived data (Schmidt et al., 2014). In our study, the seasonal acquisition timing and geographical variations did not affect the overall classification accuracy. Considering geographical variations, northern boreal and alpine plant communities do not vary considerably between latitudes in Norway (Mienna, Speed, Bendiksby, et al., 2020; Moen, 1998). This can explain why the OA did not change between sites. As far

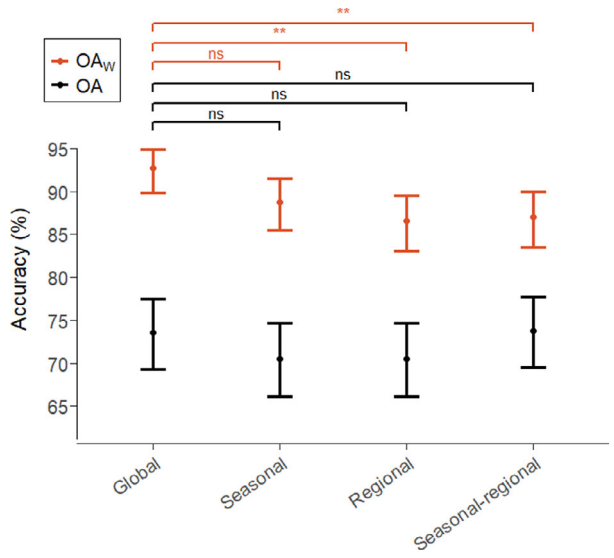

Figure 3. Overall accuracy (OA) and weighted overall accuracy (OA_W) for the global, seasonal, regional and regional-seasonal models. Vertical lines show the 95% confidence interval of each accuracy estimate. The horizontal lines show the *P*-value for the pairwise tests of each classification-set's accuracy against the global model's accuracy. Level of significance: ns, non-significant; **, ≤0.01.

as we know, no studies have investigated the optimal timing of acquiring spectral data for treeline ecotones. For vegetation types at lower elevations, multiple studies have found that the peak of the growing season is often most suitable for distinguishing plant communities (Bradter et al., 2020; Feilhauer & Schmidtlein, 2011; Schmidt et al., 2014). However, this can also depend on the vegetation type in question due to differences in phenology. Graminoid-dominated vegetation types such as wet fens and graminoid tundra can have distinct peaks in leaf-area index due to fast growth during the short growing season, while shrub and lichen tundra do not have these (Juutinen et al., 2017). Thus, different vegetation indices might be helpful to distinguish plant communities at different points in the growing season. Graminoids and shrubs are easier to distinguish early in the growing season when using vegetation indices sensitive to water absorption and plant senescence, or at the peak of the growing season using indices for photosynthetic activity and stress (Cole et al., 2014). For various arctic tundra communities, the end of the growing season has the highest spectral variability between plant communities (Beamish et al., 2017). However, the same study also found that tundra vegetation types vary little in spectral reflectance for visible and NIR light. Thus, season seem to be of a greater importance at lower elevations and latitudes for distinguishing vegetation types. The length of the seasonal phenological cycle for plant communities at higher elevations is affected by snow cover duration and lasts normally between 2 and 3 months (Vorkauf et al., 2021). The shortness of the growing season might explain why season had no influence on the classification accuracy.

Land cover classification accuracies

The classification accuracy between land cover classes varied, with the non-vegetation classes (rock, water, snow and shadow) having the highest PAs and UAs. Shadows can increase intra-class variation and thus lead to misclassifications (Lopatin et al., 2017; Lopatin et al., 2019). The rate of misclassifications is lower under cloudy conditions than in sunny conditions due to less shadows (De Sá et al., 2018). However, when balancing a trade-off between ultra-high spatial resolution from UAVs and high classification accuracies, optimal acquisition conditions is rarely an option in remote areas. To minimize the number of misclassifications in our study, we assigned shadow as a class to objects that clearly varied from neighbouring objects. This has been found to be a good alternative when one expects a shadow-effect (Milas et al., 2017).

For the vegetation classes, the accuracies varied, with wetland having the overall lowest accuracy. Wetland is often hard to map with remote sensing due to high heterogeneity and low spectral variation between wetland communities (Adam et al., 2010; Amani et al., 2017). In general, wetlands are also challenging to map consistently by field-surveys (Haga et al., 2021; Ullerud et al., 2018), so low accuracy should be expected. A possible solution for increasing the classification accuracies could be to delineate the class into wetland sub-classes found in the treeline ecotone such as open fen and bog (Halvorsen et al., 2020), or add other relevant features to the classification. The short-wave infrared region (SWIR) has been found to be important for predicting wetlands (Mcpartland et al., 2019; Meingast et al., 2014). Various topographical features such as topographical wetness index (TWI) have been found to be important for predicting wetlands, but only for specific spatial resolutions (Lidberg et al., 2020; Rasanen et al., 2014) Thus, both high spatial and spectral resolution is necessary to map wetland plant communities (Du et al., 2021). Along the ridge-snowbed gradient, snowbed had the lowest accuracy. Other remote sensing-derived features like snowmelt timing (first snow-free day of the year) could be useful for predicting snowbed (Blumentrath et al., 2016). However, snowmelt timing estimation needs remote sensing data with high temporal resolution, and this is often not correlated with high spatial resolution. Thus, predicting snowbed with UAVs is perhaps less beneficial than other remote sensing-platforms due to snowbeds often being found in remote areas and will therefore have high costs to map.

Table 4. Confusion matrix for the global Random forest model.

	Reference													
Prediction	Ridge	Xeric heath	Sub-xeric heath	Lee side	Snowbed	Tree-covered area	Wetland	Rock	Water	Snow	Shadow	Sum	UA (%)	UA_W (%)
Ridge	16	3	0	0	0	1	1	2	0	0	0	23	69.6	82.6
Xeric heath	2	9	1	0	0	0	0	0	0	0	0	12	75	100
Sub-xeric heath	2	2	9	3	0	1	0	0	0	0	0	17	52.9	82.4
Lee side	4	2	17	88	16	15	11	0	0	0	0	153	57.5	79.1
Snowbed	0	0	1	0	6	1	2	0	0	0	0	10	60	60
Tree-covered area	0	0	0	7	1	39	1	0	0	0	0	48	81.2	
Wetland	0	0	0	0	0	0	2	0	0	0	0	2	100	
Rock	2	2	0	2	2	2	1	78	3	3	0	95	82.1	
Water	1	0	1	1	0	0	0	2	52	0	2	59	88.1	
Snow	0	0	0	0	0	0	0	0	0	4	0	4	100	
Shadow	0	0	0	1	0	0	0	0	1	0	37	39	94.9	
Sum	27	18	29	102	25	59	18	82	56	7	39	462		
PA (%)	59.3	50	31	86.3	24	66.1	11.1	95.1	92.9	57.1	94.9		OA: 73.6%	
PA_W (%)	66.7	77.8	93.1	89.2	88									OA_W: 92.6%

Number of correctly classified ridge-snowbed land cover classes are shaded in dark grey. Values used to calculate the weighted accuracies (OA_w, PA_w, UA_w) are shaded in light grey. OA, overall accuracy; PA, producer's accuracy; UA, user's accuracy; PA_W, weighted PA.

In general, most of the misclassifications were between closely related classes in the ridge-snowbed gradient. In nature, plant communities that gradually blend with each other will often be poorly classified, and thus conventional classifications of plant communities are often inappropriate (Foody, 1996). As the ridge-snowbed gradient consists of discrete classes on a continuous gradient, using the weighted classification accuracies will tell us more about how the model performs. Inter-site differences for vegetation types might be caused by spectral differences due to varying edaphic and climatic conditions (Castro-Esau et al., 2006). The vegetation classes in this study can be further split up to potentially create more homogenous classes. In our study, the ridge-snowbed gradient only takes the drought risk into account, but these classes can further be divided based upon edaphic conditions represented by the basicity gradient (i.e. availability of soil nutrients along the acid–base gradient), in addition to drought risk (Halvorsen et al., 2020). Basicity often has low intra-site variation but can vary greatly between sites, possibly increasing inter-site variation due to differences in species diversity (Villoslada et al., 2020). Future studies should also take this into account to test if this changes the classification accuracies.

Feature importance

The features that increased the classification accuracy the most were all spectral. Parts of the NIR spectrum is often found to be important for classifying vegetation, and here NDVI is one of the most common vegetation indices used. Multiple studies have also found the red-edge bands to be sensitive to differences in plant physiognomy and can be useful to distinguish different vegetation types (Adamczyk & Osberger, 2015; Laba et al., 2005; Schuster et al., 2012). In our study, the red-edge band was important in improving the classification accuracy, both the mean spectral value for the band and in the vegetation index Lic3. The red-edge band seems to be important for vegetation that is adapted to drought stress (Schuster et al., 2012). In our study, the red-edge band should thus be important for the ridge-snowbed gradient due to increased risk of drought towards the ridges (Halvorsen et al., 2020).

Adding photogrammetric 3D information can improve the classification accuracy (Fraser et al., 2016; Husson et al., 2017; Sankey et al., 2017) but this is not always the case (Kattenborn et al., 2020). In our study, vertical information extracted from the normalized point cloud had intermediate importance scores. The land cover classes in the treeline ecotone should in theory not vary too much in height. The exception is lee sides that

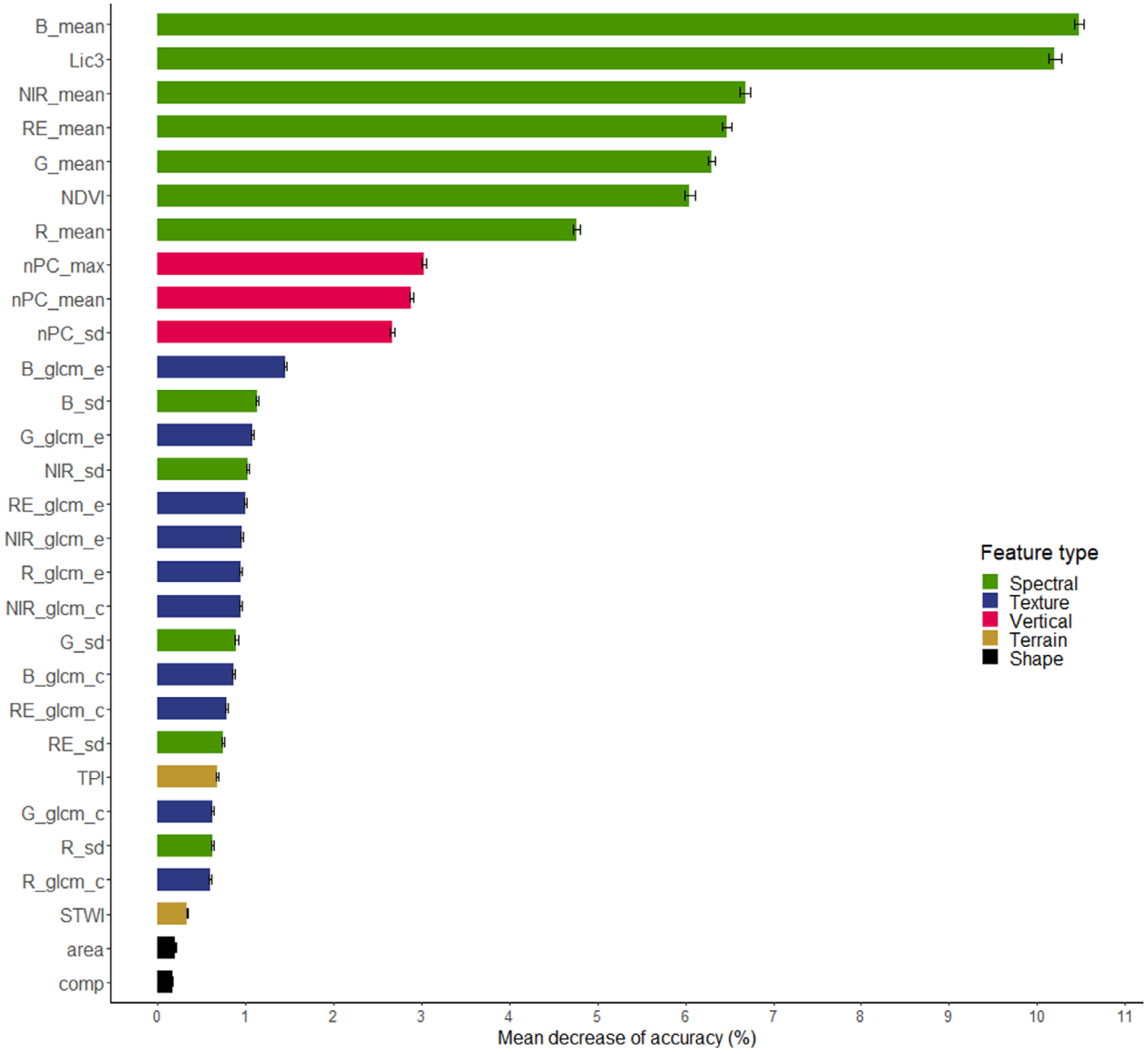

Figure 4. Feature importance derived from the global model represented as mean decrease of accuracy in percentage. The error bars show the standard errors of each feature.

can have tall shrubs like *Salix* spp. and *Juniperus communis* and trees shorter than 2 m in height. This can perhaps explain why lee sides and tree-covered areas are often misclassified. A strategy to overcome this could be to stratify segments using the normalized point cloud, where segments with points taller than a given threshold (here: 2 m) would be classified as tree-covered area (Fraser et al., 2016).

Surprisingly, the two topographical features used in this study, STWI and TPI, had overall low feature importance. Topographical features can increase prediction accuracies when classifying vegetation (Rasanen et al., 2014; Yu et al., 2006), but this can vary (Lidberg et al., 2020). Both TWI and TPI are highly affected by scale (i.e. spatial resolution of DEM) and the various settings used in the methods (e.g. drainage flow paths) (Ågren et al., 2014; Guisan et al., 1999; Mattivi et al., 2019). Thus, calculating TWI and TPI with various DEM resolutions and method settings could be a solution for investigating if these features indeed have little importance for predicting land cover classes in the treeline ecotone. Precautions should, however, be taken when interpreting feature importance scores due to feature selection biases in the classification trees (Strobl et al., 2007).

Conclusion

We found that separating observations by season and geographical region did not affect the classification accuracy compared to the global model where observations from all seasons and regions were used. This suggests that UAV data for treeline ecotone land cover maps can be acquired irrespective of timing within a growing season and geographical region. We found that spectral features related to visible, red-edge and NIR light were more important in predicting treeline ecotone land cover classes than other features. Our results can help overcoming potential time limits within the field-season when acquiring data with a goal to cover as many sites as possible.

Acknowledgements

The study was funded by The Research Council of Norway (Project no. 281066). We thank Erik Næsset and Terje Gobakken for building the data infrastructure and useful discussion about data processing. We thank Vegard Lien, Kenneth Langlie Simensen, Inger Elisabeth Hilstad and Ingegjerd Meyer for their valuable assistance during fieldwork. We thank Marie-Claude Jutras-Perreault and Jaime Candelas Bielza for processing the UAV-derived imagery before the analyses.

Data Accessibility

The data that support the findings of this study is submitted to a public repository. Questions concerning the data can be addressed to the corresponding author.

References

Adam, E., Mutanga, O. & Rugege, D. (2010) Multispectral and hyperspectral remote sensing for identification and mapping of wetland vegetation: a review. *Wetlands Ecology and Management*, **18**, 281–296.

Adamczyk, J. & Osberger, A. (2015) Red-edge vegetation indices for detecting and assessing disturbances in Norway spruce dominated mountain forests. *International Journal of Applied Earth Observation and Geoinformation*, **37**, 90–99.

Ågren, A.M., Lidberg, W., Strömgren, M., Ogilvie, J. & Arp, P.A. (2014) Evaluating digital terrain indices for soil wetness mapping – a Swedish case study. *Hydrology and Earth System Sciences*, **18**, 3623–3634.

Al-Najjar, H.A.H., Kalantar, B., Pradhan, B., Saeidi, V., Halin, A.A., Ueda, N. et al. (2019) Land cover classification from fused DSM and UAV images using convolutional neural networks. *Remote Sensing*, **11**, 18.

Amani, M., Salehi, B., Mahdavi, S., Granger, J.E., Brisco, B. & Hanson, A. (2017) Wetland classification using multi-source and multi-temporal optical remote sensing data in Newfoundland and Labrador, Canada. *Canadian Journal of Remote Sensing*, **43**, 360–373.

Batllori, E., Camarero, J.J., Ninot, J.M. & Gutiérrez, E. (2009) Seedling recruitment, survival and facilitation in alpine *Pinus uncinata* tree line ecotones. Implications and potential responses to climate warming. *Global Ecology and Biogeography*, **18**, 460–472.

Beamish, A.L., Coops, N., Chabrillat, S. & Heim, B. (2017) A phenological approach to spectral differentiation of low-arctic tundra vegetation communities, north slope, Alaska. *Remote Sensing*, **9**, 1200.

Behnamian, A., Millard, K., Banks, S.N., White, L., Richardson, M. & Pasher, J. (2017) A systematic approach for variable selection with random forests: achieving stable variable importance values. *IEEE Geoscience and Remote Sensing Letters*, **14**, 1988–1992.

Blackburn, R.C., Barber, N.A., Farrell, A.K., Buscaglia, R. & Jones, H.P. (2021) Monitoring ecological characteristics of a tallgrass prairie using an unmanned aerial vehicle. *Restoration Ecology*, **29**(S1), e13339.

Blaschke, T., Hay, G.J., Kelly, M., Lang, S., Hofmann, P., Addink, E. et al. (2014) Geographic object-based image analysis–towards a new paradigm. *ISPRS Journal of Photogrammetry and Remote Sensing*, **87**, 180–191.

Blumentrath, S., Nowell, M., Salberg, A.-B., Kermit, M., Bakkestuen, V., Erikstad, L. & Bernhardt, J.J. (2016) Sentinel4Nature: estimating environmental gradients and properties using remote sensing.

Borre, J.V., Paelinckx, D., Mücher, C.A., Kooistra, L., Haest, B., De Blust, G. et al. (2011) Integrating remote sensing in Natura 2000 habitat monitoring: prospects on the way forward. *Journal for Nature Conservation*, **19**, 116–125.

Bradter, U., O'connell, J., Kunin, W.E., Boffey, C.W.H., Ellis, R.J. & Benton, T.G. (2020) Classifying grass-dominated habitats from remotely sensed data: the influence of spectral resolution, acquisition time and the vegetation classification system on accuracy and thematic resolution. *Science of the Total Environment*, **711**, 134584.

Breiman, L. (2001) Random forests. *Machine Learning*, **45**, 5–32.

Brown, D.G. (1994) Predicting vegetation at Treeline using topography and biophysical disturbance variables. *Journal of Vegetation Science*, **5**, 641–656.

Bryn, A. & Potthoff, K. (2018) Elevational treeline and forest line dynamics in Norwegian mountain areas–a review. *Landscape Ecology*, **33**(8), 1225–1245.

Castro-Esau, K.L., Sánchez-Azofeifa, G.A., Rivard, B., Wright, S.J. & Quesada, M. (2006) Variability in leaf optical properties of Mesoamerican trees and the potential for species classification. *American Journal of Botany*, **93**, 517–530.

Cihlar, J. (2000) Land cover mapping of large areas from satellites: status and research priorities. *International Journal of Remote Sensing*, **21**, 1093–1114.

Cole, B., Mcmorrow, J. & Evans, M. (2014) Spectral monitoring of moorland plant phenology to identify a temporal window for hyperspectral remote sensing of peatland. *ISPRS Journal of Photogrammetry and Remote Sensing*, **90**, 49–58.

Dalen, L. & Hofgaard, A. (2005) Differential regional treeline dynamics in the Scandes Mountains. *Arctic Antarctic and Alpine Research*, **37**, 284–296.

De Sá, N.C., Castro, P., Carvalho, S., Marchante, E., López-Núñez, F.A. & Marchante, H. (2018) Mapping the flowering of an invasive plant using unmanned aerial vehicles: is there potential for biocontrol monitoring? *Frontiers in Plant Science*, **9**, 293.

Díaz-Varela, R.A., Iglesias, S.C., Castro, C.C. & Varela, E.R.D. (2018) Sub-metric analisis of vegetation structure in bog-heathland mosaics using very high resolution rpas imagery. *Ecological Indicators*, **89**, 861–873.

Du, B., Mao, D., Wang, Z., Qiu, Z., Yan, H., Feng, K. et al. (2021) Mapping wetland plant communities using unmanned aerial vehicle hyperspectral imagery by comparing object/pixel-based classifications combining multiple machine-learning algorithms. *IEEE Journal of Selected Topics in Applied Earth Observations and Remote Sensing*, **14**, 8249–8258.

Feilhauer, H. & Schmidtlein, S. (2011) On variable relations between vegetation patterns and canopy reflectance. *Ecological Informatics*, **6**, 83–92.

Foody, G.M. (1996) Fuzzy modelling of vegetation from remotely sensed imagery. *Ecological Modelling*, **85**, 3–12.

Fraser, R.H., Olthof, I., Lantz, T.C. & Schmitt, C. (2016) UAV photogrammetry for mapping vegetation in the low-Arctic. *Arctic Science*, **2**, 79–102.

Getzin, S., Wiegand, K. & Schöning, I. (2012) Assessing biodiversity in forests using very high-resolution images and unmanned aerial vehicles. *Methods in Ecology and Evolution*, **3**, 397–404.

Gonzalez Musso, R.F., Oddi, F.J., Goldenberg, M.G. & Garibaldi, L.A. (2020) Applying unmanned aerial vehicles (UAVs) to map shrubland structural attributes in northern Patagonia, Argentina. *Canadian Journal of Forest Research*, **50**, 615–623.

Guisan, A., Weiss, S.B. & Weiss, A.D. (1999) GLM versus CCA spatial modeling of plant species distribution. *Plant Ecology*, **143**, 107–122.

Haga, H.E.E.S., Nilsen, A.B., Ullerud, H.A. & Bryn, A. (2021) Quantification of accuracy in field-based land cover maps: a new method to separate different components. *Applied Vegetation Science*, **24**, e12578.

Hall-Beyer, M. (2017) Practical guidelines for choosing GLCM textures to use in landscape classification tasks over a range of moderate spatial scales. *International Journal of Remote Sensing*, **38**(5), 1312–1338.

Halvorsen, R., Skarpaas, O., Bryn, A., Bratli, H., Erikstad, L., Simensen, T. et al. (2020) Towards a systematics of ecodiversity: the EcoSyst framework. *Global Ecology and Biogeography*, **29**, 1887–1906.

Hamylton, S.M., Morris, R.H., Carvalho, R.C., Roder, N., Barlow, P., Mills, K. et al. (2020) Evaluating techniques for mapping Island vegetation from unmanned aerial vehicle (UAV) images: pixel classification, visual interpretation and machine learning approaches. *International Journal of Applied Earth Observation and Geoinformation*, **89**, 102085.

Harsch, M.A., Hulme, P.E., Mcglone, M.S. & Duncan, R.P. (2009) Are treelines advancing? A global meta-analysis of treeline response to climate warming. *Ecology Letters*, **12**, 1040–1049.

Hofgaard, A., Tommervik, H., Rees, G. & Hanssen, F. (2013) Latitudinal forest advance in northernmost Norway since the early 20th century. *Journal of Biogeography*, **40**, 938–949.

Hussain, M., Chen, D., Cheng, A., Wei, H. & Stanley, D. (2013) Change detection from remotely sensed images: from pixel-based to object-based approaches. *ISPRS Journal of Photogrammetry and Remote Sensing*, **80**, 91–106.

Husson, E., Reese, H. & Ecke, F. (2017) Combining spectral data and a DSM from UAS-images for improved classification of non-submerged aquatic vegetation. *Remote Sensing*, **9**, 15.

Juutinen, S., Virtanen, T., Kondratyev, V., Laurila, T., Linkosalmi, M., Mikola, J. et al. (2017) Spatial variation and seasonal dynamics of leaf-area index in the arctic tundra-implications for linking ground observations and satellite images. *Environmental Research Letters*, **12**, 095002.

Kattenborn, T., Eichel, J., Wiser, S., Burrows, L., Fassnacht, F.E. & Schmidtlein, S. (2020) Convolutional neural networks accurately predict cover fractions of plant species and communities in unmanned aerial vehicle imagery. *Remote Sensing in Ecology and Conservation*, **6**, 472–486.

Körner, C. (2012) *Alpine treelines: functional ecology of the global high elevation tree limits*. Basel: Springer.

Kullman, L. (1979) *Change and stability in the altitude of the birch tree-limit in the southern Swedish Scandes 1915–1975*. Vol. **65**. Uppsala: Acta PhytoGeographica Suecica, pp. 1–121.

Laba, M., Tsai, F., Ogurcak, D., Smith, S. & Richmond, M.E. (2005) Field determination of optimal dates for the discrimination of invasive wetland plant species using derivative spectral analysis. *Photogrammetric Engineering & Remote Sensing*, **71**, 603–611.

Lichtenthaler, H.K. (1996) Vegetation stress: an introduction to the stress concept in plants. *Journal of Plant Physiology*, **148**, 4–14.

Lidberg, W., Nilsson, M. & Ågren, A. (2020) Using machine learning to generate high-resolution wet area maps for planning forest management: a study in a boreal forest landscape. *Ambio*, **49**, 475–486.

Lopatin, J., Dolos, K., Kattenborn, T. & Fassnacht, F.E. (2019) How canopy shadow affects invasive plant species

classification in high spatial resolution remote sensing. *Remote Sensing in Ecology and Conservation*, **5**, 302–317.

Lopatin, J., Fassnacht, F.E., Kattenborn, T. & Schmidtlein, S. (2017) Mapping plant species in mixed grassland communities using close range imaging spectroscopy. *Remote Sensing of Environment*, **201**, 12–23.

Loranger, H., Zotz, G. & Bader, M.Y. (2017) Competitor or facilitator? The ambiguous role of alpine grassland for the early establishment of tree seedlings at treeline. *Oikos*, **126**, 1625–1636.

Mattivi, P., Franci, F., Lambertini, A. & Bitelli, G. (2019) TWI computation: a comparison of different open source GISs. *Open Geospatial Data, Software and Standards*, **4**, 6.

Mcpartland, M.Y., Falkowski, M.J., Reinhardt, J.R., Kane, E.S., Kolka, R., Turetsky, M.R. et al. (2019) Characterizing boreal peatland plant composition and species diversity with hyperspectral remote sensing. *Remote Sensing*, **11**, 22.

Meingast, K.M., Falkowski, M.J., Kane, E.S., Potvin, L.R., Benscoter, B.W., Smith, A.M.S. et al. (2014) Spectral detection of near-surface moisture content and water-table position in northern peatland ecosystems. *Remote Sensing of Environment*, **152**, 536–546.

Mienna, I.M., Speed, J.D.M., Bendiksby, M., Thornhill, A.H., Mishler, B.D. & Martin, M.D. (2020) Differential patterns of floristic phylogenetic diversity across a post-glacial landscape. *Journal of Biogeography*, **47**, 915–926.

Mienna, I.M., Speed, J.D.M., Klanderud, K., Austrheim, G., Næsset, E. & Bollandsås, O.M. (2020) The relative role of climate and herbivory in driving treeline dynamics along a latitudinal gradient. *Journal of Vegetation Science*, **31**, 392–402.

Mikola, J., Silfver, T. & Rousi, M. (2018) Mountain birch facilitates scots pine in the northern tree line - does improved soil fertility have a role? *Plant and Soil*, **423**, 205–213.

Milas, A.S., Arend, K., Mayer, C., Simonson, M.A. & Mackey, S. (2017) Different colours of shadows: classification of UAV images. *International Journal of Remote Sensing*, **38**, 3084–3100.

Moen, A. (1998) National atlas of Norway vegetation.

Mooney, P., Sobolowski, S. & Lee, H. (2020) Designing and evaluating regional climate simulations for high latitude land use land cover change studies. *Tellus A: Dynamic Meteorology and Oceanography*, **72**, 1–17.

Morley, P.J., Donoghue, D.N.M., Chen, J.-C. & Jump, A.S. (2018) Integrating remote sensing and demography for more efficient and effective assessment of changing mountain forest distribution. *Ecological Informatics*, **43**, 106–115.

Mottl, O., Flantua, S.G.A., Bhatta, K.P., Felde, V.A., Giesecke, T., Goring, S. et al. (2021) Global acceleration in rates of vegetation change over the past 18,000 years. *Science*, **372**, 860–864.

Mouselimis, L. (2021) SuperpixelImageSegmentation: Superpixel Image Segmentation. R package version 1.0.3.

Müllerová, J., Brůna, J., Bartaloš, T., Dvořák, P., Vítková, M. & Pyšek, P. (2017) Timing is important: unmanned aircraft vs. satellite imagery in plant invasion monitoring. *Frontiers in Plant Science*, **8**, 887.

Neuschulz, E.L., Merges, D., Bollmann, K., Gugerli, F. & Böhning-Gaese, K. (2018) Biotic interactions and seed deposition rather than abiotic factors determine recruitment at elevational range limits of an alpine tree. *Journal of Ecology*, **106**, 948–959.

Pepin, N., Bradley, R.S., Diaz, H.F., Baraër, M., Caceres, E.B., Forsythe, N. et al. (2015) Elevation-dependent warming in mountain regions of the world. *Nature Climate Change*, **5**, 424–430.

Polsby, D.D. & Popper, R.D. (1991) The third criterion: compactness as a procedural safeguard against partisan gerrymandering. *Yale Law & Policy Review*, **9**, 301–353.

Prosek, J. & Simova, P. (2019) UAV for mapping shrubland vegetation: does fusion of spectral and vertical information derived from a single sensor increase the classification accuracy? *International Journal of Applied Earth Observation and Geoinformation*, **75**, 151–162.

Puliti, S., Dash, J.P., Watt, M.S., Breidenbach, J. & Pearse, G.D. (2019) A comparison of UAV laser scanning, photogrammetry and airborne laser scanning for precision inventory of small-forest properties. *Forestry*, **93**, 150–162.

Ramtvedt, E.N., Bollandsås, O.M., Næsset, E. & Gobakken, T. (2021) Relationships between single-tree mountain birch summertime albedo and vegetation properties. *Agricultural and Forest Meteorology*, **307**, 108470.

Rasanen, A., Juutinen, S., Tuittila, E.S., Aurela, M. & Virtanen, T. (2019) Comparing ultra-high spatial resolution remote-sensing methods in mapping peatland vegetation. *Journal of Vegetation Science*, **30**, 1016–1026.

Rasanen, A., Kuitunen, M., Tomppo, E. & Lensu, A. (2014) Coupling high-resolution satellite imagery with ALS-based canopy height model and digital elevation model in object-based boreal forest habitat type classification. *ISPRS Journal of Photogrammetry and Remote Sensing*, **94**, 169–182.

Rouse, J.W., Haas, R.H., Schell, J.A. & Deering, D.W. (1974) Monitoring vegetation systems in the Great Plains with ERTS. *NASA Special Publication*, **351**, 309.

Rydsaa, J.H., Stordal, F., Bryn, A. & Tallaksen, L.M. (2017) Effects of shrub and tree cover increase on the near-surface atmosphere in northern Fennoscandia. *Biogeosciences*, **14**, 4209–4227.

3Sankey, T., Donager, J., Mcvay, J. & Sankey, J.B. (2017) UAV lidar and hyperspectral fusion for forest monitoring in the southwestern USA. *Remote Sensing of Environment*, **195**, 30–43.

Sankey, T.T., Mcvay, J., Swetnam, T.L., Mcclaran, M.P., Heilman, P. & Nichols, M. (2018) UAV hyperspectral and lidar data and their fusion for arid and semi-arid land

vegetation monitoring. *Remote Sensing in Ecology and Conservation*, **4**, 20–33.
Schmidt, T., Schuster, C., Kleinschmit, B. & Förster, M. (2014) Evaluating an intra-annual time series for grassland classification—how many acquisitions and what seasonal origin are optimal? *IEEE Journal of Selected Topics in Applied Earth Observations and Remote Sensing*, **7**, 3428–3439.
Schuster, C., Förster, M. & Kleinschmit, B. (2012) Testing the red edge channel for improving land-use classifications based on high-resolution multi-spectral satellite data. *International Journal of Remote Sensing*, **33**, 5583–5599.
Shahbazi, M., Théau, J. & Ménard, P. (2014) Recent applications of unmanned aerial imagery in natural resource management. *GIScience & Remote Sensing*, **51**, 339–365.
Speed, J.D., Austrheim, G., Hester, A.J. & Mysterud, A. (2010) Experimental evidence for herbivore limitation of the treeline. *Ecology*, **91**, 3414–3420.
Strobl, C., Boulesteix, A.-L., Zeileis, A. & Hothorn, T. (2007) Bias in random forest variable importance measures: illustrations, sources and a solution. *BMC Bioinformatics*, **8**, 25.
Stutz, D., Hermans, A. & Leibe, B. (2018) Superpixels: an evaluation of the state-of-the-art. *Computer Vision and Image Understanding*, **166**, 1–27.
Thieme, N., Bollandsas, O.M., Gobakken, T. & Naesset, E. (2011) Detection of small single trees in the forest-tundra ecotone using height values from airborne laser scanning. *Canadian Journal of Remote Sensing*, **37**, 264–274.
Tingstad, L., Olsen, S.L., Klanderud, K., Vandvik, V. & Ohlson, M. (2015) Temperature, precipitation and biotic interactions as determinants of tree seedling recruitment across the tree line ecotone. *Oecologia*, **179**, 599–608.
Ullerud, H.A., Bryn, A., Halvorsen, R. & Hemsing, L.Ø. (2018) Consistency in land-cover mapping: influence of field workers, spatial scale and classification system. *Applied Vegetation Science*, **21**, 278–288.
Ullerud, H.A., Bryn, A. & Klanderud, K. (2016) Distribution modelling of vegetation types in the boreal–alpine ecotone. *Applied Vegetation Science*, **19**, 528–540.
Villoslada, M., Bergamo, T.F., Ward, R.D., Burnside, N.G., Joyce, C.B., Bunce, R.G.H. et al. (2020) Fine scale plant community assessment in coastal meadows using UAV based multispectral data. *Ecological Indicators*, **111**, 13.
Vorkauf, M., Kahmen, A., Körner, C. & Hiltbrunner, E. (2021) Flowering phenology in alpine grassland strongly responds to shifts in snowmelt but weakly to summer drought. *Alpine Botany*, **131**, 73–88.
Wang, R. & Gamon, J.A. (2019) Remote sensing of terrestrial plant biodiversity. *Remote Sensing of Environment Nature Ecology*, **231**, 111218.
Warde, W. & Petranka, J.W. (1981) A correction factor table for missing point-center quarter data. *Ecology*, **62**, 491–494.
White, J.C., Wulder, M.A., Vastaranta, M., Coops, N.C., Pitt, D. & Woods, M. (2013) The utility of image-based point clouds for forest inventory: a comparison with airborne laser scanning. *Forests*, **4**, 518–536.
Woellner, R. & Wagner, T.C. (2019) Saving species, time and money: application of unmanned aerial vehicles (UAVs) for monitoring of an endangered alpine river specialist in a small nature reserve. *Biological Conservation*, **233**, 162–175.
Yao, H., Qin, R. & Chen, X. (2019) Unmanned aerial vehicle for remote sensing applications—A review. *Remote Sensing*, **11**, 1443.
You, Q., Cai, Z., Pepin, N., Chen, D., Ahrens, B., Jiang, Z. et al. (2021) Warming amplification over the Arctic pole and third pole: trends, mechanisms and consequences. *Earth-Science Reviews*, **217**, 103625.
Yu, Q., Gong, P., Clinton, N., Biging, G., Kelly, M. & Schirokauer, D. (2006) Object-based detailed vegetation classification with airborne high spatial resolution remote sensing imagery. *Photogrammetric Engineering & Remote Sensing*, **72**, 799–811.
Zhou, B. (2015) Image segmentation using SLIC superpixels and affinity propagation clustering. *International Journal of Science and Research*, **4**, 1525–1529.
Zvoleff, A. (2020) GLCM: calculate textures from grey-level co-occurrence matrices (GLCMs). R package version 1.6.5.

Supporting Information

Additional supporting information may be found online in the Supporting Information section at the end of the article.

Table S1. Descriptions of each study site. Map ID refers to the ID used in Figure 1.
Table S2. The merged confusion matrix for the three seasonal models (early, mid, late).
Table S3. The merged confusion matrix for the three regional models (north, middle, south).
Table S4. The merged confusion matrix for the five seasonal-regional models (early-north, early-middle, mid-middle, mid-south, late-south).

